Nucleon interaction with ^{58}Ni up to 150 MeV studied in the coupled-channels approach based on the soft-rotator nuclear structure model

Efrem Sh. Sukhovitskiĭ,[1,2] Young-Ouk Lee,[1] Jonghwa Chang,[1] Satoshi Chiba,[3] and Osamu Iwamoto[3]
[1]*Korea Atomic Energy Research Institute, Yusong, Taejon 305-600, Korea*
[2]*Radiation Physics and Chemistry Problems Institute, 220109 Minsk-Sosny, Belarus*
[3]*Japan Atomic Energy Research Institute, Tokai-mura, Naka-gun, Ibaraki-ken 319-1195, Japan*
(Received 28 March 2000; published 7 September 2000)

The soft-rotator model was applied to understand the collective nuclear structure, electromagnetic transition, and the nucleon (both neutron and proton) interaction data of ^{58}Ni in a consistent manner. It was found that the model could describe the collective level structure of ^{58}Ni, which does not exhibit the typical rotational or harmonic vibrational structure, up to excitation energy of 4.5 MeV modestly. The nucleon interaction data were described up to 150 MeV reasonably well by the coupled-channels method with a coupling scheme constructed consistent to the nuclear structure of ^{58}Ni.

PACS number(s): 25.40.−h, 21.60.Ev, 24.10.Eq

I. INTRODUCTION

The ^{58}Ni nucleus has attracted a good deal of attention from the applicational point of view since it is a component of the structure materials of nuclear reactors and D-T fusion devices, i.e., steels in which the overall portion of ^{58}Ni exceeds 10% usually. Furthermore, for the design of the accelerator-driven nuclear wastes transmutation facilities [1], not only neutron- but also proton-induced cross sections of ^{58}Ni are requested for incident energies up to 150 MeV.

On the fundamental side, ^{58}Ni is considered normally as a vibrational nucleus, and nucleon interaction cross section calculations, using coupled-channels or distorted-wave Born approximation (DWBA) formalism, are performed involving the harmonic vibrational model. However, the ^{58}Ni nucleus does not exhibit a level spectrum characteristic to the harmonic vibration; the degeneracy of the two-phonon triplet is broken considerably, showing that the anharmonicity effect is large in this nucleus. Furthermore, the energy splitting of the yrast 0^+, 2^+, 4^+, and 6^+ levels is very irregular to be considered as harmonic vibrational states. Therefore, the calculation of nucleon interaction cross sections cannot ignore the effect of such anharmonicity, which implies that the nuclear structure information is very important for a correct understanding of the interaction cross sections of this nucleus.

In the present work, we employ the soft-rotator model to desribe the collective level structure of the ^{58}Ni nucleus. This model was found to be very successful in describing the nuclear structure, nucleon interaction, and $B(E2)$ transitions for both very light (^{12}C) [2] and heavy (actinide) [3] nuclei. It is therefore a matter of big interest to see whether or not the soft-rotator model [4,5], frequently employed for rotational nuclides successfully, is applicable in the mass region of ^{58}Ni where the collective structure is more vibrational in nature. To realize our purpose we used a very small equilibrium deformation, but a very large softness to the quadrupole deformation, so that the ground-state band could describe the corresponding band in the U(5) symmetry limit of the IBM-1 [6]. Until now, no consistent attempts have been given to describe the low-lying collective level structure and nucleon scattering data of ^{58}Ni in such a unified framework. The purpose of this work is to carry out such an analysis, intending to use the results for a high-energy nuclear data evaluation for ^{58}Ni.

II. COUPLED-CHANNELS FORMALISM BASED ON THE SOFT-ROTATOR MODEL

The soft-rotator model was developed as an extension of the Davydov-Chaban model [7] which takes account of the β vibration in nonaxial soft rotational nuclei. Here, the word ''soft'' denotes the possibility of stretching during the rotation. The present version of the soft-rotator model includes the nonaxial quadrupole, octupole, and hexadecapole deformations, and the β_2, β_3, and γ vibrations [3–5]. The soft-rotator model and its application as a base for creating a reliable and self-consistent coupling scheme, built on the wave functions of the soft-rotator nuclear model Hamiltonian, for coupled-channels (CC) optical model calculations are described elsewhere [8]. Here, we give a brief description of the model to make this paper reasonably self-contained.

In this model we assume that excited states observed in even-even nonspherical nuclei can be described as a combination of rotation, β-quadrupole, and octupole vibrations, and γ-quadrupole vibration. Instant nuclear shapes that correspond to such excitations can be presented in a body-fixed system:

$$R(\theta',\varphi')=R_0\left\{1+\sum_{\lambda\mu}\beta_{\lambda\mu}Y_{\lambda\mu}\right\}=R_0\left\{1+\beta_2\left[\cos\gamma Y_{20}(\theta',\varphi')+\frac{1}{\sqrt{2}}\sin\gamma[Y_{22}(\theta',\varphi')+Y_{2-2}(\theta',\varphi')]\right]\right.$$

 ©2000 The American Physical Society

$$+\beta_3\left[\cos\eta Y_{30}(\theta',\varphi')+\frac{1}{\sqrt{2}}\sin\eta[Y_{32}(\theta',\varphi')+Y_{3-2}(\theta',\varphi')]\right]+\beta_{40}Y_{40}(\theta',\varphi')$$
$$+\sum_{\mu=2,4}\beta_{4\mu}[Y_{4\mu}(\theta',\varphi')+Y_{4-\mu}(\theta',\varphi')]\Bigg\}. \tag{1}$$

The Hamiltonian $\hat{H}$ of the soft-rotator model corresponding to the above nuclear shape can be formed according to the Pauli quantization technique [9]:

$$\hat{H}=\frac{\hbar^2}{2B_2}\left\{\hat{T}_{\beta_2}+\frac{1}{\beta_2^2}\hat{T}_\gamma\right\}+\frac{\hbar^2}{2}\hat{T}_r+\frac{\hbar^2}{2B_3}\hat{T}_{\beta_3}+\frac{\beta_{20}^4}{\beta_2^2}V(\gamma)$$
$$+V(\beta_2)+V(\beta_3), \tag{2}$$

where the kinetic energy operators for the vibrational motions are given as

$$\hat{T}_{\beta_2}=-\frac{1}{\beta_2^4}\frac{\partial}{\partial\beta_2}\left(\beta_2^4\frac{\partial}{\partial\beta_2}\right), \tag{3}$$

$$\hat{T}_\gamma=-\frac{1}{\sin 3\gamma}\frac{\partial}{\partial\gamma}\left(\sin 3\gamma\frac{\partial}{\partial\gamma}\right), \tag{4}$$

$$\hat{T}_{\beta_3}=-\frac{1}{\beta_3^3}\frac{\partial}{\partial\beta_3}\left(\beta_3^3\frac{\partial}{\partial\beta_3}\right). \tag{5}$$

The symbol $V(x)$ denotes the confining potential for a vibration of type x (where $x=\gamma$, β_2, or β_3), taken to be of the harmonic oscillator form which is parametrized by the state-dependent equilibrium deformation and elasticity constant (or softness parameter). The symbol $\hat{T}_r$ represents the operator of deformed nuclear rotational energy expressed in terms of the angular momentum operator $\hat{I}_i$ and principal moments of inertia,

$$\hat{T}_r=\sum_{i=1}^{3}\frac{\hat{I}_i^2}{J_i}=\sum_{i=1}^{3}\frac{\hat{I}_i^2}{J_i^{(2)}+J_i^{(3)}+J_i^{(4)}}$$
$$=\frac{1}{4B_2\beta_2^2}\sum_{i=1}^{3}\frac{\hat{I}_i^2}{j_i^{(2)}+a_{32}j_i^{(3)}+a_{42}j_i^{(4)}}, \tag{6}$$

where $j_i^{(\lambda)}=J_i^{(\lambda)}/4B_\lambda\beta_\lambda^2$ and $a_{\lambda 2}=(B_\lambda/B_2)(\beta_\lambda/\beta_2)^2$. Here $J_i^{(\lambda)}$ stands for the principal moments of inertia in the direction of ith axis in the body-fixed system due to quadrupole, octupole, and hexadecapole deformations depending on $\lambda=2$, 3, and 4, respectively. The symbol $\hat{I}_i$ denotes the projection of the angular momentum operator on the ith axis of the body-fixed coordinate, β_{20} denotes the quadrupole equilibrium deformation parameter at the ground state (g.s.), and B_λ denotes the mass parameter for multipolarity of λ. The eigenfunctions Ψ of the Hamiltonian operator (2) are defined in the space of six dynamical variables: $0\leqslant\beta_2<\infty$, $-\infty<\beta_3<\infty$, $n\pi/3\leqslant\gamma\leqslant(n+1)\pi/3$, $0\leqslant\theta_1\leqslant 2\pi$, $0\leqslant\theta_2\leqslant\pi$, and $0\leqslant\theta_3<2\pi$, with the volume element $d\tau=\beta_2^4\beta_3^3|\sin 3\gamma|d\beta_2 d\beta_3 d\gamma d\theta_1\sin\theta_2 d\theta_2 d\theta_3$. Here $\beta_\lambda^2=\Sigma_\mu\beta_{\lambda\mu}\beta_{\lambda\mu}^*$ is the measure of nucleus deformation with multipolarity λ. After an appropriate choice of the Hamiltonian parameters, this procedure gives us the rotational-vibrational energy spectra for the low-lying collective levels and the wave functions which are used to calculate the coupling strengths to be employed in the coupled-channels analysis as will be described immediately below.

As usual, multipoles of deformed nuclear potential are determined, expanding it in Taylor series, considering $[\Sigma_{\lambda\mu}\beta_{\lambda\mu}Y_{\lambda\mu}(\theta',\varphi')]$ to be small:

$$V(R)=V(R_i)+\sum_{t=1}^{max}\frac{\partial^t V}{\partial R^t}\bigg|_{R=R_i}\frac{R_i^t}{t!}\left(\sum_{\lambda\mu}\beta_{\lambda\mu}Y_{\lambda\mu}(\theta',\varphi')\right)^t. \tag{7}$$

The essence of the coupled-channels formalism based on the soft-rotator model is in the account of the enhancement of the coupling strengths as compared with the rigid-rotor model which arises because the dynamic variables appearing in the expansion of the deformed potential are averaged over the appropriate wave functions Ψ which are solutions of the Hamiltonian, Eq. (2), describing rotational-vibrational states of nonaxial deformed deformable nuclei. Such an enhancement is equal to $\langle i|\beta_\lambda^t|f\rangle/\beta_{\lambda\,\mathrm{g.s.}}^t$ and this ratio is usually greater than unity, as nuclei are rotating with increasing velocity for collective states with higher spins I and thus are increasingly stretched due to centrifugal forces so that equilibrium deformations $\beta_{\lambda I\tau}$ for states with higher spins I are greater than the equilibrium g.s. deformation $\beta_{\lambda\,\mathrm{g.s.}}$. As the deformation potential energy $V(\beta_\lambda)$ of the soft-rotator model in terms of nuclear softness μ_λ is considered to be $\sim(1/\mu_\lambda^4)(\beta_\lambda-\beta_{\lambda\,\mathrm{g.s.}})^2$, the coupling enhancement is larger for nuclei with larger softness μ_λ and vanishes for nuclei with small μ_λ. Such enhancements are different for different combinations of initial $|i\rangle$ and final $|f\rangle$ states [which are eigenfunctions of Eq. (2)], and also depend on the powers of potential expansion t. In this way, the soft-rotator model takes account of the nuclear softness, predicting the redistribution of the coupling strength, i.e., the particle current between the channels, which in turn changes the estimates of direct level excitation cross sections compared with the rigid-rotor of harmonic-vibrational model.

The optical potential is taken to be a standard form:

$$V(r)=-V_R f_R(r)+i\left\{4W_D a_D \frac{d}{dr} f_D(r)-W_V f_V(r)\right\}$$
$$+\left(\frac{\hbar}{\mu_\pi c}\right)^2 (V_{SO}+iW_{SO})\frac{1}{r}\frac{d}{dr} f_{SO}(r)\boldsymbol{\sigma}\cdot\mathbf{L}+V_{Coul}(r), \tag{8}$$

with the form factors given as

$$f_i=\left[1+\exp\left(\frac{r-R_i}{a_i}\right)\right]^{-1}, \quad R_i=r_i A^{1/3},$$
$$i=R,\ V,\ D, \quad \text{and } SO. \tag{9}$$

For the reasons mentioned above we need the potential expansion expressed with evident dependences on deformations. In the case of the Coulomb potential $V_{Coul}(r)$ such an expansion with evident dependences of deformations becomes possible as we follow the suggestion of Bassel *et al.* [10], using a multipole expansion of the Coulomb potential V_{Coul} up to the second order in $\Sigma\beta_{\lambda\mu}Y_{\lambda\mu}$ for a charged ellipsoid with a uniform charge density within the Coulomb radius R_C and zero outside. However, the Coulomb potential used in the present work included some modifications [2]. The spherical term of it was calculated, taking into account the diffuseness of the charge distribution. Our model involves quadrupole, octupole, and hexadecapole instant nuclear deformations; i.e., the Coulomb expansion of the potential can in principle give additional coupling strength between collective states with an angular momentum transfer of 0–8. However, in the Coulomb expansion used in this model, we truncate the dynamic square terms which lead to a zero angular momentum transfer. This is equivalent to introducing a dynamic negative deformation β_{00} in the radial expansion given in Eq. (1),

$$\beta_{00}=-\sum_\lambda (-1)^\lambda \sqrt{\frac{2\lambda+1}{4\pi}}(\beta_\lambda\otimes\beta_\lambda)_{00}, \tag{10}$$

which is required as a condition to conserve the nuclear volume, i.e., the nuclear charge [9]. This correction is necessary to have the right asymptotic behavior for the spherical term of the Coulomb potential which must be equal to $ZZ'e^2/r$. The additional coupling due to the Coulomb potential was obtained in the same manner as for the nuclear one [8] with deformed radii as described above.

The subscripts $i=R,\ V,\ D$, and SO in Eqs. (3) and (4) denote the real volume, imaginary volume, imaginary surface, and real spin-orbit potentials, respectively. The strength of these potentials is assumed to have the following form:

$$V_R=V_R^0+V_R^1E_p+V_R^2E_p^2+(-1)^{Z'+1}C_{viso}(A-2Z)/A$$
$$+C_{Coul}ZZ'/A^{1/3},$$
$$W_D=W_D^0+W_D^1E_p+(-1)^{Z'+1}C_{wiso}(A-2Z)/A,$$
$$W_V=W_V^0+W_V^1E_p,$$
$$W_{SO}=W_{SO}^0+W_{SO}^1E_p, \tag{11}$$

where Z', Z are charges of incident particle and target nucleus, and A the target mass number. The symbol E_p denotes the energy of the projectile and potential slopes W_D^1 and W_V^1 may change at $E_p=E_{change}$. Noticeable energy losses due to collective level excitation of the ^{58}Ni nuclei as compared with the nucleon incident energies involved in the analysis request the dependence of local optical potential for different channels, which was taken into account for diagonal potential elements as

$$V_{if}=V(E_p-E_i)$$

and for nondiagonal elements as

$$V_{if}=V\left(E_p-\frac{E_i+E_f}{2}\right),$$

where i and f denote initial and final channels, while E_i and E_f the corresponding level energies. As we intend to analyze neutron and proton scattering data simultaneously, our potential contains a term $C_{Coul}ZZ'/A^{1/3}$ describing the Coulomb correction to the real optical potential and isospin terms $(-1)^{Z'+1}C_{viso}(A-2Z)/A$ added to real and $(-1)^{Z'+1}C_{wiso}(A-2Z)/A$ added to imaginary surface potentials.

III. ESTIMATION OF SOFT-ROTATOR NUCLEAR MODEL HAMILTONIAN PARAMETERS DESCRIBING LOW-LYING ^{58}Ni COLLECTIVE LEVELS

The SHEMMAN code [11] was used to adjust the soft-rotator nuclear model Hamiltonian parameters, allowing the description of the experimentally observed low-lying collective levels of the ^{58}Ni nucleus. Initial assignment of the soft-rotator model quantum numbers to the experimentally observed low-lying collective levels of ^{58}Ni was done in our standard approach. We considered yrast levels with spins and parities $J^\pi=0_1^+$ (g.s.), 2_1^+(1.454 MeV), and 4_1^+(2.459 MeV) to be the members of the ground-state rotational band with $K\simeq 0$, $^{58}\text{Ni}=n_{\beta_2}=n_\gamma=0$. Second $J^\pi=2_2^+$(2.775 MeV) and first $J^\pi=3_1^+$(3.420 MeV) levels were assigned as members of the $K\simeq 2$, $n_{\beta_2}=n_{\beta_3}=n_\gamma=0$ band. This allowed us to find initial soft-rotator Hamiltonian parameters describing the chosen experimental levels. The initially adjusted Hamiltonian parameters made possible the assignment of the soft-rotator model quantum numbers to other observed levels, considered as levels of the g.s. $K\simeq 0$, $n_{\beta_2}=n_{\beta_3}=n_\gamma=0$; $K\simeq 2$, $n_{\beta_2}=n_{\beta_3}=n_\gamma=0$; and $K\simeq 0$, $n_{\beta_2}=1$, $n_{\beta_3}=n_\gamma=0$ bands. After ^{58}Ni experimental levels were assigned in this way, the final nuclear Hamiltonian parameters were adjusted using the SHEMMAN code [11].

The rotational or vibrational structure is not very prominent in the case of the ^{58}Ni nuclide; nevertheless, we could describe the first five low-lying collective levels and some others lying above, necessary for creating a coupling scheme of CC calculations, with an accuracy of about 10%. For most of these levels the accuracy is better, except the levels con-

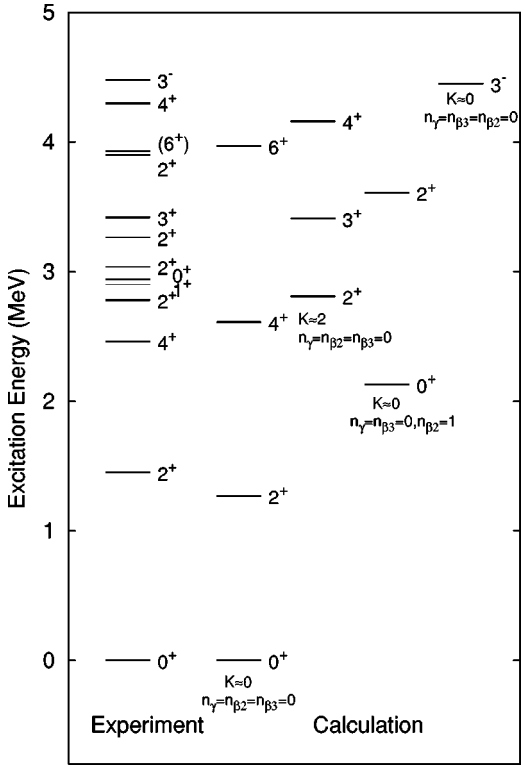

FIG. 1. Comparison of the experimental and calculated level schemes. Thick lines show experimental levels described by the soft-rotator model. Note that above 3.5 MeV excitation energy, due to a lack of space and not to overcrowd the figure, we demonstrate only those experimental levels that are predicted by our model.

sidered as first levels of the $K\simeq 0$, $n_{\beta_2}=1$, $n_{\beta_3}=n_\gamma=0$ band with $J^\pi=0_2^+$(2.942 MeV) and 2_5^+(3.898 MeV). For instance the first excited 2_1^+ level with measured energy of 1.454 MeV is predicted by the model at 1.269 MeV, the 4_1^+ level ($E_x=2.459$ MeV) is predicted at 2.615 MeV, the 2_2^+ level ($E_x=2.775$ MeV) at 2.806 MeV, and the 3_1^+ level ($E_x=3.420$ MeV) at 3.412 MeV. The model predicts the experimentally measured level with 3.934 MeV excitation energy, the spin of which is not assigned, to be the $J^\pi=6_1^+$ level of the g.s. band, with a predicted energy of 3.968 MeV. The second $J^\pi=0_2^+$ level with energy 2.942 MeV was described as the head of the $K\simeq 0$, $n_{\beta_2}=1$, $n_{\beta_3}=n_\gamma=0$ band. However, the predicted energy 2.134 MeV is not in good agreement with experimental value of 2.942 MeV. The level with $J^\pi=2^+$ of this band predicted with energy 3.615 MeV is assigned to the experimental $J^\pi=2_5^+$ (3.898 MeV) one.

TABLE I. The nuclear Hamiltonian parameters which are adjusted to reproduce the experimental level scheme.

$\hbar\omega_0=1.2470$		
$\mu_{\beta_{20}}=1.9095$	$\mu_{\gamma_0}=0.4000$	$\gamma_0=0.6272$
$a_{32}=0.0001$	$\gamma_4=0.14410$	$\delta_4=0.6971$
$a_{42}=0.01486$	$\mu_\epsilon=0.4707$	
$\eta=0.14556$	$\delta_n=7.4301$	

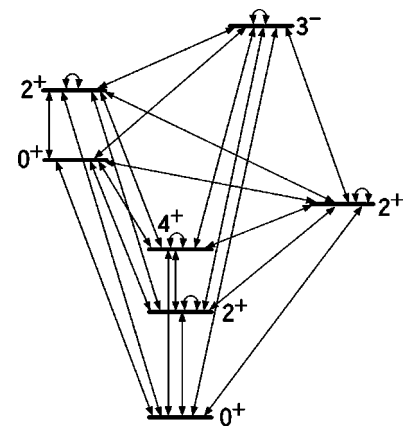

FIG. 2. Coupling scheme employed in the present calculation. Arrows show the coupling used in the parameter search procedure.

The level with spin and parity $J^\pi=1_1^+$ (2.901 MeV) is not of a collective nature and we were not trying to describe it. The level with $J^\pi=4^+$ found at 4.299 MeV is described as the member of $K\simeq 2$, $n_{\beta_2}=n_{\beta_3}=n_\gamma=0$ for which the model predicts a 4.157 MeV excitation energy. The negative parity level $J^\pi=3_1^-$(4.474 MeV) with predicted energy 4.452 MeV is described as the member of the negative parity $K\simeq 0$, $n_{\beta_2}=n_{\beta_3}=n_\gamma=0$ band, the energy of which is described by energy splitting for symmetric and antisymmetric β_3 oscillator function solutions, determining positive and negative parity collective states of the soft-rotator model accordingly [3]. Figure 1 demonstrates the comparison of experimental and predicted ^{58}Ni level schemes. Please note that the level scheme of ^{58}Ni becomes very dense above excitation energy of 3.5 MeV, and our model was unable to describe many of the levels in this energy region. However, most of them are considered to be of a noncollective nature. Thus, we demonstrate only those levels that are predicted by our model in order not to overcrowd Fig. 1 above 3.5 MeV excitation energy.

The nuclear Hamiltonian parameters allowing the demonstrated level prediction are given in Table I. Here the physical meanings of the parameters are explained briefly: the μ_x's ($x=\beta_{20}$, γ_0, ϵ) denote the nuclear softness parameters for the β_2, γ, and β_3 vibrations, respectively; $a_{\lambda 2}=(B_\lambda/B_2)(\beta_\lambda/\beta_2)^2$ where $\lambda=3$ or 4 as explained previously; η, γ_4, and δ_4 determine the nonaxiality of octupole and hexadecapole deformations; $2\delta_n$ gives the energy splitting of a doubly degenerate level in the octupole vibration due to the tunneling effect; and the $\hbar\omega_0$ normalizes the overall scale of the predicted energy levels. The symbols β_{20} and γ_0 give the equilibrium quadrupole deformations at the ground state. We considered the octupole deformation to be transformed as $\beta_3=\beta_2\epsilon$ which is in direct proportion to the increase of β_2 due to centrifugal forces caused by nuclear rotations. It is shown in Ref. [12] that this enables one to reproduce various patterns of level-energy intervals observed experimentally for positive and negative parity bands of even-even nuclei. The equilibrium g.s. octupole deformation is given as $\beta_{30}=\beta_{20}\epsilon_0$. The deformation parameters β_{20}, ϵ_0, and β_4 are the parameters in our approach to be

TABLE II. Experimental scattering data involved in the CC optical analysis.

Reference	Projectile	Energy (MeV)	Spin, parity, energy of the excited level $0^+(0.0)$	$2^+(1.454)$	$3^-(4.475)$
Smith *et al.* [15]	Neutron	4.5	a	a	
		5.0	a	a	
		5.5	a	a	
		5.9	a	a	
		6.5	a	a	
		7.14	a	a	
		7.5	b	b	
		8.029	a	a	
		8.399	a	a	
		9.06	b	b	
		9.5	a	a	
Guss *et al.* [16]	Neutron	7.904	b	b	
		9.958	b	b	
		11.952	b	b	
		13.941	b	b	
Tutubalin *et al.* [17]	Neutron	14.7	b		
Perdoni *et al.* [18]	Neutron	16.934	b	b	
Yamanouti *et al.* [19]	Neutron	24.0	b	b	b
Tesmer and Schmidt [25]	Proton	20.0	a	a	
Van Hall *et al.* [26]	Proton	20.4	a	a	
		24.6	a	a	a
Ridley and Turner [20]	Proton	30.3	b		
Stovall and Hintz [21]	Proton	39.7		b	b
Blumberg *et al.* [22,23]	Proton	40.0	b	b	b
Fulmer *et al.* [24]	Proton	61.4	b		
Sakaguchi *et al.* [27]	Proton	65.0	a		

[a]Data used for potential parameter adjustment.
[b]Data used for comparison only.

determined from an analysis of reaction data and will be given later (Table III) with the optical potential parameters obtained simultaneously.

One can see from Table I that ^{58}Ni demonstrates a large softness $\mu_{\beta_{20}}=1.9095$. It is consistent with the well-known fact that nuclei with N and Z in the vicinity of magic numbers can be considered spherical for the g.s. and are deformed in excited states; for our model that means that such ^{58}Ni nuclei are very soft to β_2 deformations.

IV. ESTIMATION OF THE OPTICAL POTENTIAL PARAMETERS

Nuclear wave functions of the soft-rotator model with the adjusted nuclear Hamiltonian parameters, given in Table I, were used to construct the coupling among seven collective ^{58}Ni levels [0^+(g.s.), 2_1^+(1.454 MeV), 4_1^+(2.459 MeV), 2_2^+(2.775 MeV), 0_2^+(2.942 MeV), 2_5^+(3.898 MeV), and 3_1^-(4.475 MeV)] in the CC calculations using the OPTMAN code [11,13]. Preliminary numerical results showed that the inclusion of additional levels influences the numerical results by much less than experimental errors. Levels coupled in current calculations and the coupling scheme are presented in Fig. 2. Each pair of levels having the same parity and levels themselves are coupled by all possible even multipoles with angular momentum transfer up to $8\hbar$ and by odd multipoles with angular momentum transfer up to $7\hbar$ for pairs of levels with different parity. The Coulomb interaction enhances the coupling in all the pairs of levels except between 0^+(g.s.) and 0_2^+(2.942 MeV) states (as square terms which lead to Coulomb potential zero multipoles were truncated), so these levels were coupled only by the nuclear potential. We must emphasize that levels from various bands are coupled in our model not only with the ground-state band,

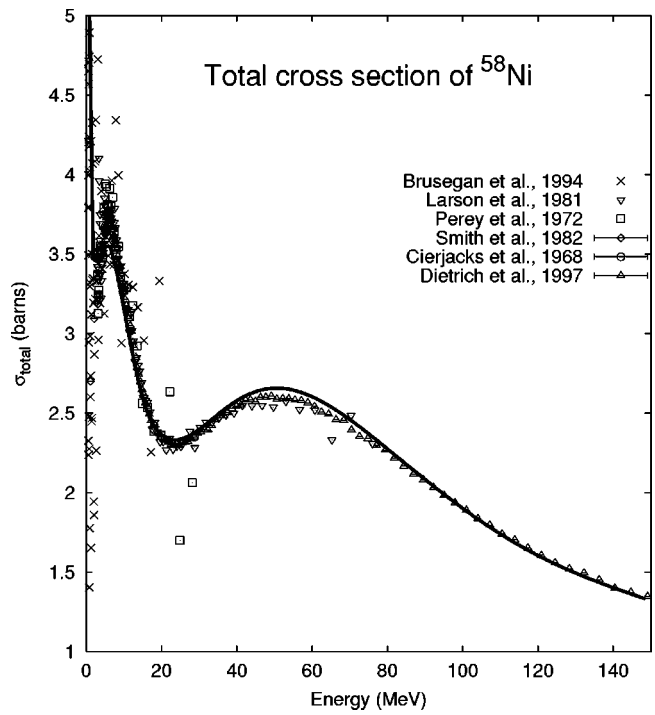

FIG. 3. Comparison of experimental and calculated ^{58}Ni total neutron cross sections up to 150 MeV incident energy. Solid line: present calculation.

but also with each other, without any additional assumptions. Such a feature is absent in most of the previous analyses.

Experimental data used for the optical potential search were taken from the EXFOR database [14]. The following experimental neutron scattering data were involved in the current analysis: angular distribution measurements of neutrons scattered on the g.s. and the first 2^+ excited level for 11 incident energies from 4.5 to 10 MeV of Smith *et al.* [15]; analogous experimental results for incident neutron energies 7.904, 9.958, 11.952, and 13.941 MeV of Guss *et al.* [16]; elastic scattering angular distribution measured for 14.7 MeV incident energy by Tutubalin *et al.* [17]; scattered neutron angular distribution measurements for the g.s. and the first 2^+ excited level for 16.934 MeV incident energy of Perdoni *et al.* [18]; and experimental scattered neutrons angular distribution data for the g.s. and the first 2^+ and 3^- levels at 24 MeV incident energy of Yamanouti *et al.* [19].

Proton interaction data are rather scarce, so we can use the 30.3 MeV incident proton elastic scattering angular distributions measurement of Ridley and Turner [20]; data on inelastic proton scattering angular distributions by the first 2^+ and 3^- levels at 39.7 MeV by Stovall and Hintz [21]; 40 MeV incident proton elastic scattering angular distributions measured by Blumberg *et al.* [22], supplemented by measurements of angular distributions for the first 2^+ and 3^- levels for the same incident energy by Fricke *et al.* [23]; and the elastic scattering angular distribution measured for 61.4 MeV incident energy by Fulmer *et al.* [24]. We can use for comparison the scattering data [25–27] for 20, 20.4, 24.6, and 65 MeV incident energies, which have no reliable experimental errors in EXFOR because they were compiled by reading the graphs presented in publications.

Detailed information about the data used in the CC analysis can be found in Table II. The evaluated neutron strength functions $S_{l=0,1}$ and ^{58}Ni total neutron interaction cross section σ_{tot}, based on Refs. [15,28], up to 20 MeV incident neutron energies and the natural Ni total cross section corrected for other Ni isotope contamination (accounting for the fact that σ_{tot} is proportional to $A^{2/3}$ for different isotopes) were also used. The data from Ref. [29–32] covering the entire region of incident neutron energies necessary were also used in the optical potential adjustment. One can see that we did not include scattered angular distribution data for nucleon interaction energies below 7 MeV in the adjustment. As checked, for such incident energies we could not guarantee that the compound interaction contribution to angular distributions is less than the experimental errors and can be neglected. For lower energies, the energy loss even for the first 2_1^+(1.454 MeV) excited level decreases the nucleon en-

TABLE III. The optical potential parameters allowing the best fit of the experimental data. Strength and incident energy E in MeV; radii and diffusenesses in fm.

$V_R = 52.33 - 0.394E + 0.00107E^2$		
$W_D = \begin{cases} 4.40 + 0.126E & E \leqslant 25.75 \\ 7.645 - 0.0577(E - 25.75) & E > 25.75 \end{cases}$		
$W_V = \begin{cases} 1.16 + 0.057E & E \leqslant 25.75 \\ 2.628 + 0.0547(E - 25.75) & E > 25.75 \end{cases}$		
$V_{SO} = 4.80$	$W_{SO}^0 = 0.0$	$W_{SO}^1 = 0.0$
$r_R = 1.2275$	$a_R = 0.593 + 0.00115E$	
$r_D = 1.1371$	$a_D = \begin{cases} 0.509 + 0.00253E & E \leqslant 25.75 \\ 0.5741 & E > 25.75 \end{cases}$	
$r_V = 1.0967$	$a_V = 0.493 + 0.00426$	
$r_{SO} = 1.1232$	$a_{SO} = 0.660$	
$r_C = 1.2437$	$a_C = 0.573$	
$C_{Cuol} = 0.493$	$C_{viso} = 0.85$	$C_{wiso} = 3.25$
$\beta_{20} = 0.0788$	$\beta_{30} = \beta_{20}\epsilon_0 = 0.0805$	$\beta_4 = 0.0142$

ergy in outgoing scattering channels to the energy region with resonance structure (experimentally observed in the total cross section for neutrons; see Fig. 3) which can influence the results of the potential search. We therefore could assume that the interaction of nucleons with ^{58}Ni for experimental data involved for optical potential search proceeds only via the direct mechanism, which can be described by the optical model.

Using one of the OPTMAN code [11,13] options, the optical potential parameters were searched by minimizing the quantity χ^2 defined by

$$\chi^2=\frac{1}{N+M+2}\left[\sum_{i=1}^{N}\frac{1}{K_i}\sum_{j=1}^{K_i}\left(\frac{d\sigma_{ij}/d\Omega_{calc}-d\sigma_{ij}/d\Omega_{expt}}{\Delta\sigma_{ij}/d\Omega_{expt}}\right)^2 + \sum_{i=1}^{M}\left(\frac{\sigma_{tot_{cal_i}}-\sigma_{tot_{eval_i}}}{\Delta\sigma_{tot_{eval_i}}}\right)^2+\sum_{i=0}^{1}\left(\frac{S_{l_{cal_i}}-S_{l_{eval_i}}}{\Delta S_{l_{eval_i}}}\right)^2\right],$$

where N is the number of experimental scattering data sets, K_i the number of angular points in each data set, and M the number of energies, for which the experimental neutron total cross section is involved. During the optical parameter search, the parameters of the nuclear Hamiltonian were fixed except for μ_{γ_0}; it was impossible to determine this Hamiltonian parameter by analyzing the level scheme alone, since no levels with $n_\gamma \geqslant 1$ are observed in our analysis of ^{58}Ni level scheme due to our assignment.

V. RESULTS AND DISCUSSION

A. Coupled-channels analysis

The adjusted optical potential parameters, allowing the best fit to the the experimental data, are presented in Table III. It is evident that the total neutron cross section data for ^{58}Ni [15,28–32] in the energy region from 3 to 150 MeV (Fig. 3) and available experimental neutron and proton scattering data (Figs. 4–9) are described fairly well by the present model in a consistent manner. The overall χ^2 is 4.5, which means that the experimental data are described on average within approximately two experimental errors. We consider such a quality of description acceptable, yet some comments are necessary.

One can see (Fig. 6) that our calculations underestimate the angular distributions of neutrons with incident energy 5.9 MeV, scattered on the 2^+(1.454 MeV) level. For the same reason the predicted elastic scattering for this incident energy underestimates the experimental values, predicting a deeper valley for about 135° scattering angles (Fig. 4). It proves, as discussed above, that the contribution of the compound scattering mechanism for such energies could not be neglected. This was the reason not to include experimental scattering data for incident energies below 7.5 MeV in the optical potential parameter search.

Experimental angular distributions of protons scattered by 2^+(1.454 MeV) and especially 3^-(4.474 MeV) levels [21,23], which are measured for almost the same incident energies 39.7 and 40 MeV accordingly, are in contradiction

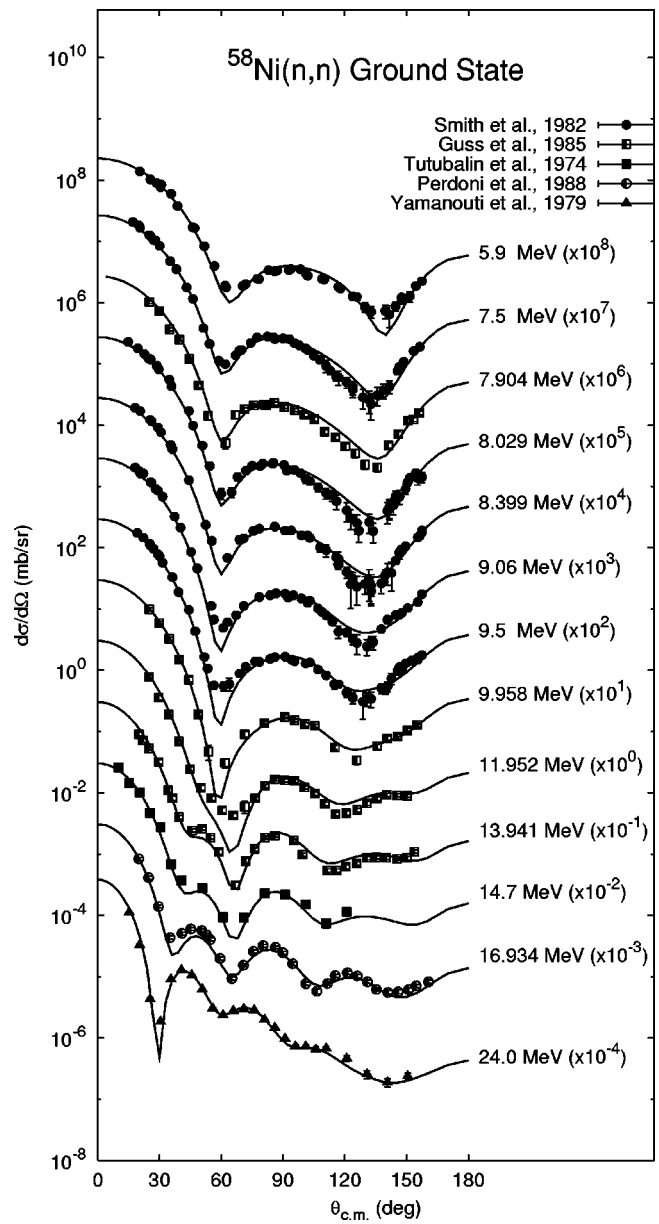

FIG. 4. Comparison of experimental and calculated angular distributions for neutrons elastically scattered from ^{58}Ni. Solid lines: present calculation.

(see Figs. 7 and 9). We relied on Stovall and Hintz's data [21] in the potential parameters search due to the reason mentioned above. This determines lower predicted angular distribution values for 3^- level excitation as compared with [23] for 40 MeV and [26] for 24.6 MeV incident energies.

Above we mentioned the redistribution of the coupling strength in different channels without any additional assumptions as the inherent feature of the (CC) approach builds on wave functions of the soft-rotator Hamiltonian. The ''equilibrium'' quadrupole ^{58}Ni deformation β_{20} was found to be 0.0788 in this analysis, which gives an ''effective'' deformation of 0.195, when averaged by β_2 oscillation functions, resulting in a 0.925 fm ''effective'' deformation length for direct excitation of the 2^+(1454 MeV) level. The latter value can be compared with 0.9 fm used

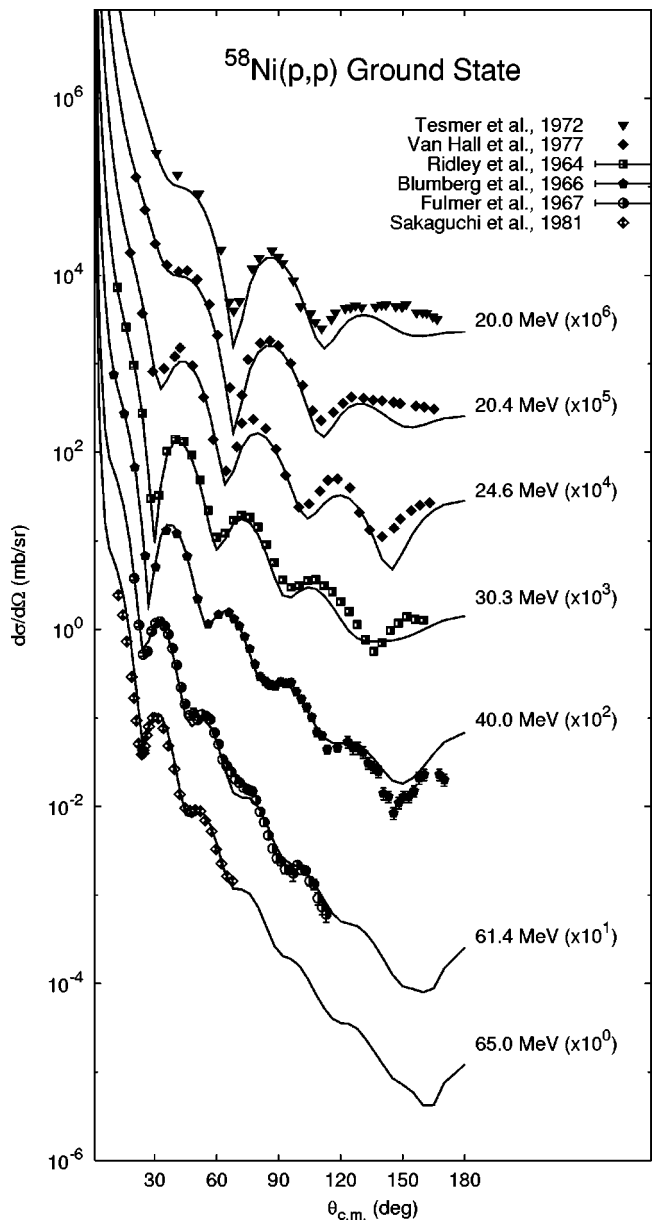

FIG. 5. Comparison of experimental and calculated angular distributions for protons elastically scattered from ^{58}Ni. Solid lines: present calculation.

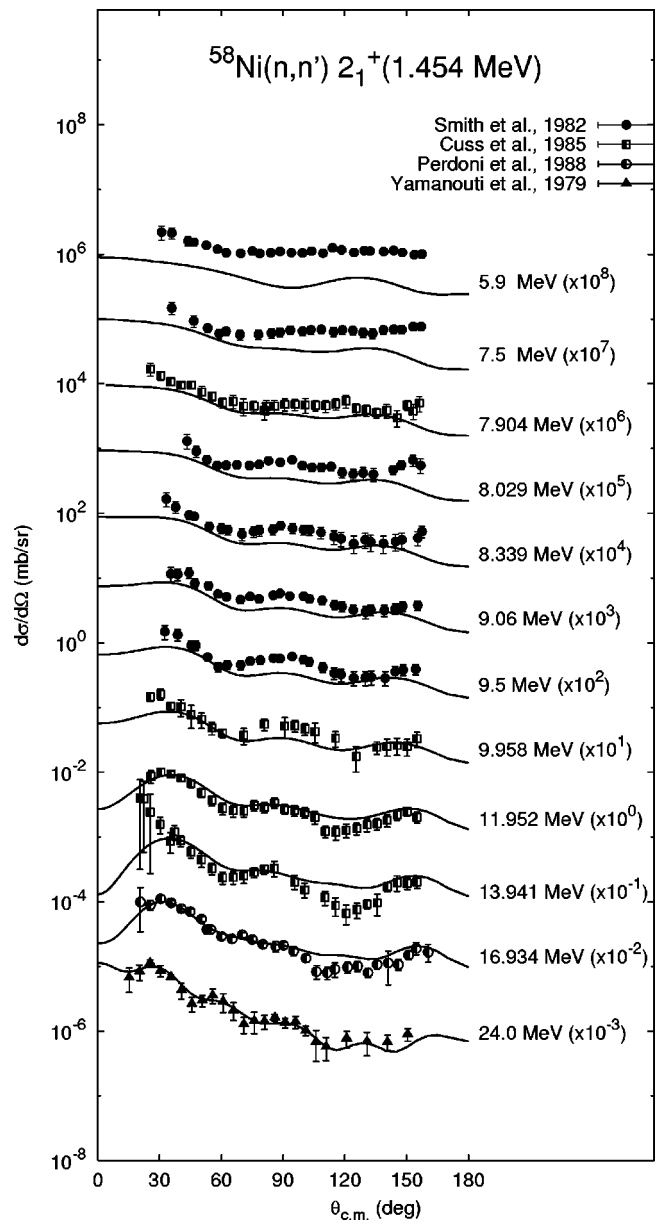

FIG. 6. Comparison of experimental and calculated angular distributions for neutrons scattered to the 2^+ (1.454 MeV) level of ^{58}Ni. Solid lines: present calculation.

in the harmonic oscillator model analysis of ^{58}Ni angular distributions [33]. This fact shows the softness of ^{58}Ni to such a degree of freedom, a feature ignored in the frequently employed rigid-rotator model. The result of our $\langle 0^+|\beta_2^2|0_2^+\rangle$ value determining one-step excitation of the 0_2^+ (2.942 MeV) level is 15% lower than $\langle 0^+|\beta_2^2|2_1^+\rangle$, while $\langle 0^+|\beta_2|2_1^+\rangle\langle 2_1^+|\beta_2|0_2^+\rangle$ determining the two-step excitation strength is 35% lower. This results in the lower coupling strength decreasing the predicted 0_2^+ level excitation value compared with the model assuming a constant β_2 value, which requests for such models an appropriate determination of β_2 for each pair of channels. This is what we call the redistribution of the coupling strength, which leads to the redistribution of nucleon current in a different channel without additional assumptions. It is the result of the stretching of a soft rotating ^{58}Ni nucleus due to rotations incorporated in the present model.

The volume integrals per nucleon for the real central part calculated from the present potential are plotted in Fig. 10 where it is compared to the same quantity calculated from global potentials: the neutron and proton potentials of Walter and Guss [34] and proton potential of Schwandt *et al.* [35]. It is evident that the present results are consistent with these widely accepted potentials. Especially the present proton result gives a smooth transition from the lower-energy region (where it is in excellent agreement with the Walter-Guss potential) to the higher-energy region to agree with the potential of Schwandt *et al.* In the overlapping region of the potentials of Walter and Guss and Schwandt *et al.*, these two

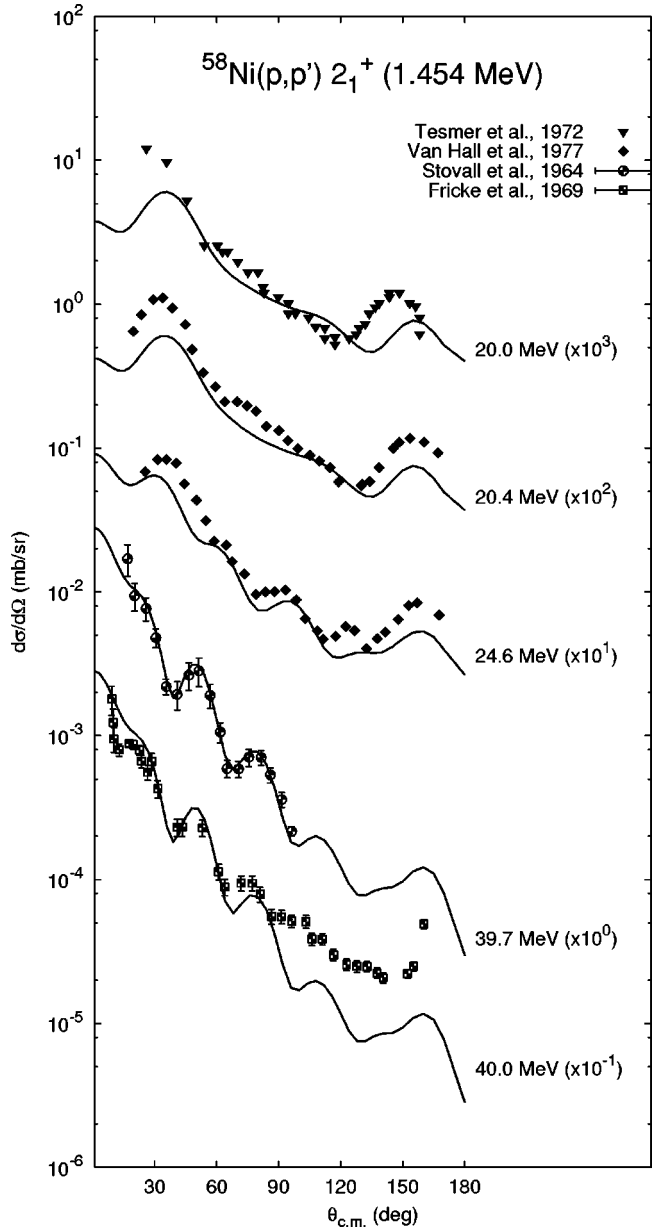

FIG. 7. Comparison of experimental and calculated angular distributions for protons scattered to the 2^+ (1.454 MeV) level of ^{58}Ni. Solid lines: present calculation.

potentials have a slight inconsistency with each other because the proton potential of Schwandt *et al.* is lower than the Walter-Guss neutron potential in spite of the fact that the Coulomb correction must enhance the proton potential noticeably compared to the neutron one. Here we must recall that the Walter-Guss potential was determined by considering the scattering (both of neutron and proton) and neutron total cross section data simultaneously as was done in the present work, while the potential of Schwandt *et al.* was determined by taking account of the proton scattering, mostly analyzing power, data alone. Therefore we consider it to be acceptable to have an agreement with the Walter-Guss potential while having a slight disagreement with the potential of Schwandt *et al.* at the low-energy region. Furthermore, the

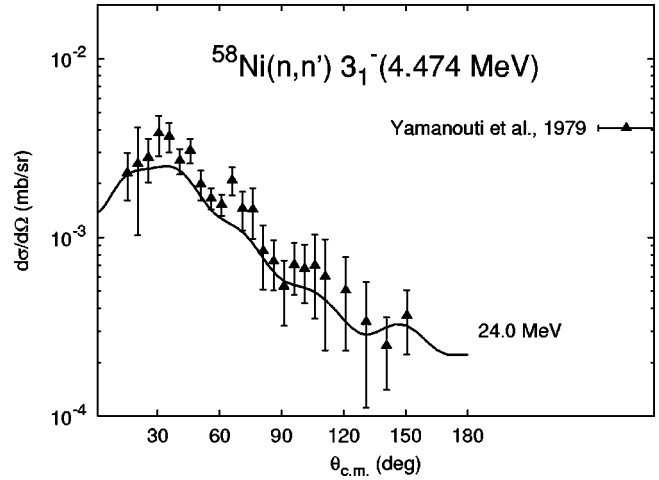

FIG. 8. Comparison of experimental and calculated angular distribution for neutrons scattered to the 3^- (4.475 MeV) level of the ^{58}Ni. Solid lines: present calculation.

difference in the present neutron and proton potentials, caused mainly by the Coulomb correction term, lies in a reasonable range, which agrees also with that of the Walter-Guss potential. We did not compare here the volume integrals for the imaginary potential because the global potentials considered here are for spherical model calculations while the present potential can be smaller than them due to the fact that the coupling to the excited levels is considered explicitly.

Finally we give a rough estimate of the uncertainties of the deduced parameters. In our case the χ^2 value has a flat

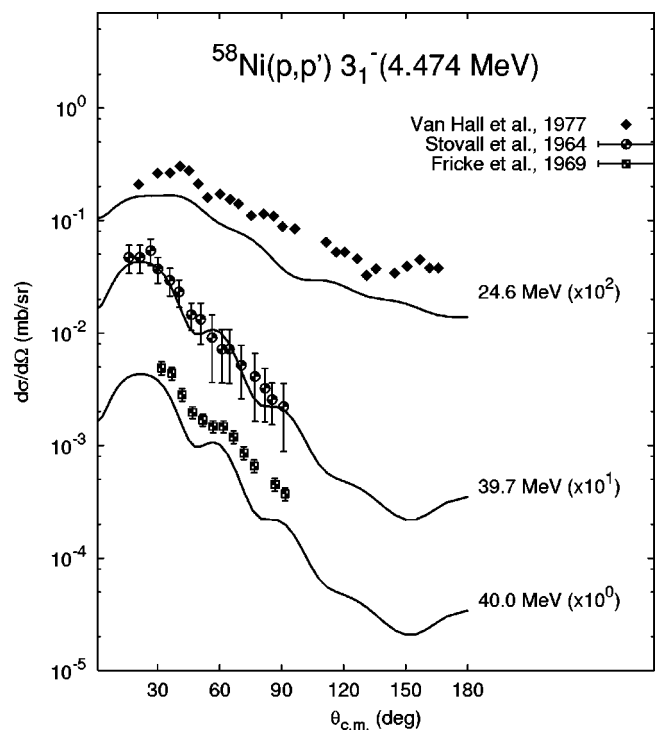

FIG. 9. Comparison of experimental and calculated angular distributions for protons scattered to the 3^- (4.475 MeV) level of the ^{58}Ni. Solid lines: present calculation.

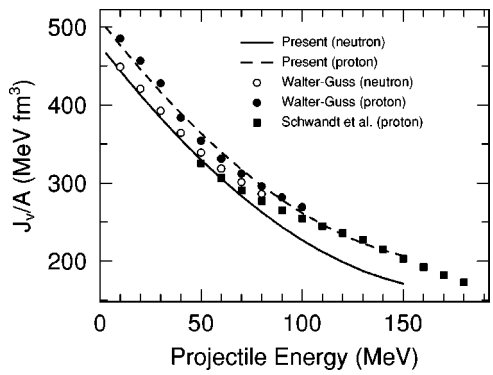

FIG. 10. Volume integrals per nucleon of the real central part of the present potential (solid lines for neutrons and dashed line for protons) compared to that of the Walter-Guss neutron (open circles) and proton (solid circles) potentials and that of the proton potential of Schwandt *et al.* (solid squares).

minimum valley, so the potential uncertainties were estimated as deviations of the parameters which are required to give a noticeable change in χ^2 for at least one individual energy angular distribution. In this approach the uncertainty of V_R was estimated as 0.5 MeV, those of W_D and W_V as 0.2 MeV, that of r_R as 0.003 fm, those of r_D, r_V, and r_C as 0.005 fm, and those of the diffuseness parameters as 0.005 fm.

B. $B(E2)$ data

The γ-transition probability $B(E\lambda)$ can also be calculated by the soft-rotator model. The leading term in $B(E2)$ is proportional to the square of an integral over the β_2 variable [8,2] guiding the enhancement of the coupling strength. Higher terms can be also taken into consideration (see Ref. [9]). As in the case of coupling in the CC calculation, the probabilities of the γ transition between different levels are enhanced differently compared with the rigid-rotator model. The absolute value of $B(E2)$ depends on the equilibrium deformation values which were determined by fitting to the reaction data as described above.

The $B(E2;0^+(\text{g.s.})\rightarrow 2_1^+)$ transition probability was calculated as 0.0134 $e^2\,\text{b}^2$ with the account of inner dynamic variables up to square terms. The experimental value is evaluated to be 0.0131 $e^2\,\text{b}^2$ [36]. The experimentally measured upper limit value for the $B(E2;4_1^+\rightarrow 2_1^+)$ transition probability is 0.057 $e^2\,\text{b}^2$ [36], which is equal to 0.028 $e^2\,\text{b}^2$ in our calculations. Considering the fact that no parameter was adjusted to calculate this quantity, our prediction is in good agreement with the experimental value.

VI. CONCLUDING REMARKS

The soft-rotator nuclear model and CC method with a coupling based on the soft-rotator model wave functions were applied to analyze available ^{58}Ni experimental total, nucleon scattering, collective level structure, and electromagnetic transition rates in a consistent fashion. It was found that the model gives a modest success in describing the collective low-lying level structure of ^{58}Ni which exhibits neither the typical rotational nor the vibrational spectra, while the nucleon interaction data were described reasonably well up to 150 MeV. It is recommended that such an approach be used for the analysis of the nucleon interaction with other nuclei in this mass region to validate the usefulness of the present method. The results of the present work can be used for the evaluation of high-energy nuclear data of ^{58}Ni for application purposes such as accelerator-driven transmutation technology.

ACKNOWLEDGMENTS

The authors would like to thank Dr. Akira Hasegawa of the JAERI nuclear data center for his support and Dr. Jeong-Yeon Lee of the KAERI nuclear data evaluation laboratory for helpful comments on this work. One of the authors (E.Sh.S.) is grateful to the Korea Ministry of Science and Technology, Korea Institute of Science and Technology Evaluation Planning for providing financial support, and Korea Atomic Energy Research Institute for offering the opportunity to stay at KAERI and for the hospitality of KAERI Nuclear Data Evaluation Laboratory team, which made this work possible for him.

[1] S. Matsuura, Nucl. Phys. **A654**, 417c (1999).
[2] E. Sh. Sukhovitskiĭ, Y. V. Porodzinskiĭ, S. Chiba, O. Iwamoto, and Y. V. Porodzinskiĭ, Nucl. Phys. **A640**, 147 (1998).
[3] Y. V. Porodzinskiĭ and E. Sh. Sukhovitskiĭ, Yad. Fiz. **59**, 263 (1996) [Phys. At. Nucl. **59**, 244 (1996)].
[4] Y. V. Porodzinskiĭ and E. Sh. Sukhovitskiĭ, Yad. Fiz. **53**, 64 (1991) [Sov. J. Nucl. Phys. **53**, 41 (1991)].
[5] Y. V. Porodzinskiĭ and E. Sh. Sukhovitskiĭ, Yad. Fiz. **54**, 1538 (1991) [Sov. J. Nucl. Phys. **54**, 941 (1991)].
[6] F. Iachello and A. Arima, *The Interacting Boson Model* (Cambridge University Press, Cambridge, England, 1987).
[7] A. S. Davydov and A. A. Chaban, Nucl. Phys. **20**, 499 (1960).
[8] S. Chiba, O. Iwamoto, Y. Yamanouti, M. Sugimoto, M. Mizumoto, K. Hasegawa, E. Sh. Sukhovitskiĭ, Y. V. Porodzinskiĭ, and Y. Watanabe, Nucl. Phys. **A624**, 305 (1997).
[9] J. M. Eisenberg and W. Greiner, *Nuclear Models* (North-Holland, Amsterdam, 1970).
[10] R. H. Bassel, R. M. Drisko, and G. R. Satchler, Oak Ridge National Laboratory Report No. ORNL-3240, 1962.
[11] E. Sh. Sukhovitskiĭ, Y. V. Porodzinskiĭ, O. Iwamoto, S. Chiba, and K. Shibata, Report No. JAERI-Data/Code 98-019, JAERI, 1998.
[12] A. Y. Dzyublik and V. Y. Denisov, Yad. Fiz. **56**, 30 (1993) [Phys. At. Nucl. **56**, 303 (1993).
[13] E. Sh. Sukhovitskiĭ, O. Iwamoto, S. Chiba, and K. Shibata, Report No. JAERI-Data/Code 99-028, JAERI, 1999.
[14] H. D. Lemmel, Report No. IAEA-NDS-1 Rev.7, Vienna, 1996.
[15] A. B. Smith, P. T. Guenter, J. F. Whalen, and S. Chiba, J. Phys. G **18**, 624 (1992); for approved data see Report No. ANL-NDM-120, 1991.

[16] P. P. Gus *et al.*, Nucl. Phys. **A438**, 187 (1985).
[17] A. I. Tutubalin *et al.*, in *Proceedings of the 2nd National Soviet Conference on Neutron Physics*, Kiev, 1973, edited by L. N. Usachev (F.E.I., Obninsk, 1974), Vol. 3, p. 62.
[18] R. S. Perdoni *et al.*, Phys. Rev. C **38**, 2052 (1988).
[19] Y. Yamanouti *et al.*, in Proceedings of the International Conference on Nuclear Cross Sections for Technology, Knoxville, Tennessee, 1979, NBS Spec. Publ. No. 594, 1980, p. 146.
[20] B. W. Ridley and J. F. Turner, Nucl. Phys. **58**, 497 (1964).
[21] T. Stovall and N. M. Hintz, Phys. Rev. **135**, B350 (1964).
[22] L. N. Blumberg, E. E. Cross, A. Von Der Woude, A. Zucker, and R. H. Bassel, Phys. Rev. **147**, 812 (1966).
[23] M. P. Fricke, E. E. Cross, and A. Zucker, Phys. Rev. **181**, 1565 (1969).
[24] C. B. Fulmer, J. B. Ball, A. Scott, and M. L. Whitten, Phys. Rev. **163**, 1153 (1967).
[25] J. R. Tesmer and F. H. Schmidt, Phys. Rev. C **5**, 864 (1972).
[26] P. J. Van Hall *et al.*, Nucl. Phys. **A261**, 63 (1977).
[27] H. Sakaguchi, M. Nakamura, K. Hatanaka, and T. Noro, Phys. Lett. **99B**, 92 (1981).
[28] A. Brusegan *et al.*, in Proceedings of the International Conference on Nuclear Data for Science and Technology, Gatlinburg, 1994 (unpublished), p. 224.
[29] S. Cierjacks *et al.*, Report No. KFK-1000 (Suppl. 1), 1968.
[30] F. G. Perey, T. A. Love, and W. E. Kinney, Report No. ORNL-4823, 1972.
[31] D. C. Larson, J. A. Harver, and N. W. Hill, Report No. ORNL-5787, 1981.
[32] F. S. Dietrich *et al.*, in Proceedings of the International Conference on Nuclear Data for Science and Technology, Trieste, 1997 (unpublished), Vol. 1, p. 402.
[33] A. J. Koning, J. P. Delaroche, and O. Bersillon, Report No. ENC-RX-97-047, Netherlands Energy Research Foundation ECN, 1997.
[34] R. L. Walter and P. P. Guss, in Proceedings of the International Conferences on Nuclear Data for Basic and Applied Science, Santa Fe, 1985, p. 1079.
[35] P. Schwandt, H. O. Meyer, W. W. Jacobs, A. D. Bacher, S. E. Vigdor, M. D. Kaitchuck, and T. R. Donoghue, Phys. Rev. C **26**, 55 (1982).
[36] S. Raman, C. H. Malarkey, W. T. Milner, C. W. Nestor, Jr., and P. H. Stelson, At. Data Nucl. Data Tables **36**, 1 (1987).